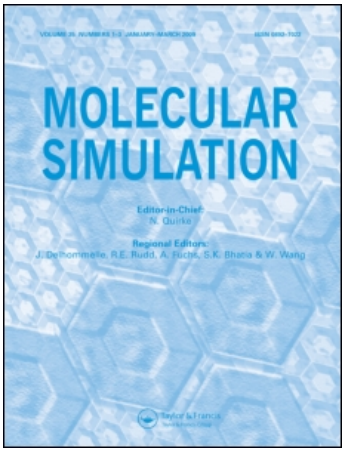

Molecular Simulation
Publication details, including instructions for authors and subscription information:
http://www.informaworld.com/smpp/title~content=t713644482

Cell size dependence of orientational order of uniaxial liquid crystals in flat slit

Toshiki Mima[a]; Tetsu Narumi[a]; Shun Kameoka[a]; Kenji Yasuoka[a]
[a] Department of Mechanical Engineering, Keio University, Yokohama, Japan

To cite this Article Mima, Toshiki , Narumi, Tetsu , Kameoka, Shun and Yasuoka, Kenji(2008) 'Cell size dependence of orientational order of uniaxial liquid crystals in flat slit', Molecular Simulation, 34: 8, 761 — 773
To link to this Article: DOI: 10.1080/08927020802256058
URL: http://dx.doi.org/10.1080/08927020802256058

Molecular Simulation
Vol. 34, No. 8, July 2008, 761–773

Taylor & Francis
Taylor & Francis Group

Cell size dependence of orientational order of uniaxial liquid crystals in flat slit

Toshiki Mima*, Tetsu Narumi, Shun Kameoka and Kenji Yasuoka

Department of Mechanical Engineering, Keio University, Yokohama, Japan

(*Received 18 March 2008; final version received 5 June 2008*)

In order to investigate the ordered structure of nematic liquid crystal molecules confined in a nanoslit, we carried out a classical molecular dynamics simulation of uniaxial prolate Gay–Berne particles in a flat, structureless slit at several temperatures. When the slit gap is so small that the system is not assumed as the bulk, particles in the slit possess orientationally ordered structures different from ones in the bulk. The weak spacial orientational correlation existed when the temperature corresponded to the isotropic phase in the bulk system. The first order isotropic–nematic phase transition was not clearly observed and the transitional phenomenon of the creation and annihilation of the uniaxial domains were observed. These results revealed that the ordered structure depends on the number of particles, in other words, cell size, and that the system with 100,000 or more particles gives reasonable results of an infinitely wide slit. The number of particles is converted into up to 220 particles of the length of the base.

Keywords: liquid crystal; molecular simulation; confined

PACS: 61.30.Cz; 47.57.Lj; 68.08. − p

1. Introduction

The order of a liquid crystal (LC) phase depends on the shapes of molecules in the system. LC molecules have been successfully applied to display devices, and LC molecules and LC phases have been investigated regardless of the complexity of the molecule and the degree of the order [1–3]. Recently, it has been proven that dendrons realise various LC phases: first, wedge-shaped dendrons form disk-like or sphere micelles, then a columnar phase or phases with 3D lattice symmetries [4–6]. The self-assembly of the dendron LC is expected to be applied photonic devices and nanoporous catalysts. On the other hand, even in the simple nematic phase, an insight has been developed. De Miguel and Martín del Río [7] carried out the molecular dynamics simulation of hard ellipsoids with super-imposed square-well attractions in order to investigate the re-entrant behaviour of the nematic phase. They have successfully depicted the phase diagram containing the re-entrant nematic phase and implied that the LC in the smectic phase can lose the long-range order of the centres of mass so that the free energy is minimised upon compressing.

Not only the LC molecules themselves, but also the interaction between the LC molecules and the interface have been studied [8–10]. Recently, the properties of molecules confined in submicron- or nano-sized spaces are being actively studied along with the development of microfabrication techniques [11–14]: water in a graphite slit or carbon nanotube has been very widely investigated [15–18]. LC molecules in a nano-sized confinement are also expected to possess properties which are different from those in the bulk system. They have shown different characteristics [19–24]. A lot of simulated research has been carried out to investigate the order of the LC molecules confined in a several nanopore shapes in the past decade [25–31]. However, it has been implied that the LC molecules in a thin space may possess a weak, but long-range orientational order, and many particles are needed to simulate a more realistic system [32].

In this study, we investigated the uniaxial nematogen Gay–Berne particles in the thin, flat, structureless slit whose slit gap equals about six particles. Specifically, the orientational order depending on the number of the particles or the cell size is discussed in detail. In Section 2, the simulation cell, the interaction between two ellipsoids, the ellipsoid–wall interaction and the definition of the physical quantities are described. In Section 3, the results and discussion are presented. First, the fluidity of the centres of mass of the particles is examined, then the orientational properties are concentrated on the following section. The conclusion follows in Section 4.

2. Methods

2.1 System

In order to investigate the prolate nematic LC in the slit, uniaxial, prolate Gay–Berne particles are confined in a thin slit [31]. The slit is comprised of two flat, structureless

*Corresponding author. Email: t_mima@z8.keio.jp

ISSN 0892-7022 print/ISSN 1029-0435 online

DOI: 10.1080/08927020802256058
http://www.informaworld.com

walls that are parallel to each other. The z-axis is perpendicular to the slit. The shape of the base on the xy plane remains square. The periodic boundary condition is imposed in the x- and y-directions. Gay–Berne particles are simulated at a constant pressure, constant temperature and constant slit gap ensemble; the number of particles, N, the element of the pressure tensor parallel to slit, $P_{\|}$, the temperature, T, and the slit gap, h, are fixed in the simulation. $N = 1000$, 9000, 16,000, 64,000 and 100,000 are investigated at $T = 1.20$, 1.15, 1.10, 1.05 and 1.00. Additionally, $N = 169{,}000$ is investigated at $T = 1.20$, 1.15 and 1.10. $P_{\|}$ is set to 4.5 and h is set to 6.0 through all the simulations. The following statement should be considered: Gay–Berne particles in our study exhibit isotropic behaviour at the $T = 1.20$ and 1.15, nematic behaviour at the $T = 1.10$ and 1.05, and uniaxial solid behaviour at the $T = 1.00$ when they are in the bulk system at the pressure of 4.5 [33].

The equations of motion of the $NhP_{\|}T$ ensemble have been used in our simulation [31,34]. The Andersen's barostat is attached to the x- and y-directions of the positional equations. In other words, the slit gap is fixed and the area, $A = L^2$, can stretch and shrink, where L is the length of a edge of the base. In order to keep the temperature constant, Nosé's thermostat is applied to both the translation of centres of mass and the rotation of the orientational vectors. The slit does not explicitly interact any particles with heat.

2.2 Interaction

The interaction between two uniaxial, prolate particles is described by the Gay–Berne potential [35],

$$\phi_{\mathrm{GB}}(\boldsymbol{r}_{ij}, \boldsymbol{e}_i, \boldsymbol{e}_j) = 4\epsilon(\hat{\boldsymbol{r}}_{ij}, \boldsymbol{e}_i, \boldsymbol{e}_j) \cdot \left[\left(\frac{\sigma_0}{r_{ij} - \sigma(\hat{\boldsymbol{r}}_{ij}, \boldsymbol{e}_i, \boldsymbol{e}_j) + \sigma_0} \right)^{12} - \left(\frac{\sigma_0}{r_{ij} - \sigma(\hat{\boldsymbol{r}}_{ij}, \boldsymbol{e}_i, \boldsymbol{e}_j) + \sigma_0} \right)^{6} \right], \tag{1}$$

$$\epsilon(\hat{\boldsymbol{r}}_{ij}, \boldsymbol{e}_i, \boldsymbol{e}_j) = \epsilon_0 \left(\frac{1}{\sqrt{1 - \chi^2 (\boldsymbol{e}_i \times \boldsymbol{e}_j)^2}} \right)^{\nu} \cdot \Psi(\hat{\boldsymbol{r}}_{ij}, \boldsymbol{e}_i, \boldsymbol{e}_j, \chi')^{\mu}, \tag{2}$$

$$\sigma(\hat{\boldsymbol{r}}_{ij}, \boldsymbol{e}_i, \boldsymbol{e}_j) = \frac{\sigma_0}{\sqrt{\Psi(\hat{\boldsymbol{r}}_{ij}, \boldsymbol{e}_i, \boldsymbol{e}_j, \chi)}}, \tag{3}$$

where $\boldsymbol{r}_{ij} = \boldsymbol{q}_i - \boldsymbol{q}_j$, which is the positional vector between the ith and jth centres of mass of the ellipsoids, $\boldsymbol{q}_i$ and $\boldsymbol{q}_j$, respectively, and $\hat{\boldsymbol{r}}_{ij}$ is the normalised positional vector. $\boldsymbol{e}_i$ is the orientation vector of the ith ellipsoid, which corresponds to its long axis. The magnitude of $\boldsymbol{e}_i$ is unity. σ_0, ϵ_0, ν, μ, χ and χ' are parameters. Ψ is the function for anisotropy,

$$\Psi(\hat{\boldsymbol{r}}_{ij}, \boldsymbol{e}_i, \boldsymbol{e}_j; a) = 1 - \frac{a}{2} \left[\frac{(\hat{\boldsymbol{r}}_{ij} \cdot \boldsymbol{e}_i + \hat{\boldsymbol{r}}_{ij} \cdot \boldsymbol{e}_j)^2}{1 + a \boldsymbol{e}_i \cdot \boldsymbol{e}_j} + \frac{(\hat{\boldsymbol{r}}_{ij} \cdot \boldsymbol{e}_i - \hat{\boldsymbol{r}}_{ij} \cdot \boldsymbol{e}_j)^2}{1 - a \boldsymbol{e}_i \cdot \boldsymbol{e}_j} \right], \quad a = \chi, \chi'. \tag{4}$$

In this paper, $\epsilon_0 = 1$, $\sigma_0 = 1$. χ is set to 0.8, which corresponds to 3.0 in the axial ratio. $\nu = 1$, $\mu = 2$ and $\chi' \simeq 0.382$; the nematic phase can occur with this choice of parameters [33].

There are various descriptions of interactions between a Gay–Berne ellipsoid and a wall [25,26,30,36]. We define the potential by imposing anisotropy in a Lennard-Jones 9-3 potential [31,37]:

$$\phi_{\mathrm{wall}}(z_i, e_{i,z}; z_{\mathrm{w}}) = \frac{2\pi}{3} \epsilon_{\mathrm{w}}(e_{i,z}) \cdot \left[\frac{2}{15} \left(\frac{\sigma_{0\mathrm{w}}}{|z_i - z_{\mathrm{w}}| - \sigma_{\mathrm{w}}(e_{i,z}) + \sigma_{0\mathrm{w}}} \right)^9 - \left(\frac{\sigma_{0\mathrm{w}}}{|z_i - z_{\mathrm{w}}| - \sigma_{\mathrm{w}}(e_{i,z}) + \sigma_{0\mathrm{w}}} \right)^3 \right], \tag{5}$$

where z_i is the position in the z-direction of ith particle, $e_{i,z}$ is the z component of the ith orientation and z_{w} is the position of the wall. As in the Gay–Berne potential, ϵ_{w}, σ_{w} and Ψ_{w} are functions for the anisotropy,

$$\epsilon_{\mathrm{w}}(e_{i,z}) = \epsilon_{0\mathrm{w}} \left(\frac{1}{\sqrt{1 - \chi_{\mathrm{w}}^2 (1 - 2e_{i,z}^2)}} \right)^{\nu_{\mathrm{w}}} \cdot \Psi_{\mathrm{w}}(e_{i,z}; \chi'_{\mathrm{w}})^{\mu_{\mathrm{w}}}, \tag{6}$$

$$\sigma_{\mathrm{w}}(e_{i,z}) = \frac{\sigma_{0\mathrm{w}}}{\sqrt{\Psi_{\mathrm{w}}(e_{i,z}; \chi_{\mathrm{w}})}}, \tag{7}$$

$$\Psi_{\mathrm{w}}(e_{i,z}; a) = 1 - \frac{2a e_{i,z}^2}{1 - a(1 - 2e_{i,z}^2)}, \quad a = \chi_{\mathrm{w}}, \chi'_{\mathrm{w}}. \tag{8}$$

In this paper, $\sigma_{0\mathrm{w}} = \sigma_0$, $\epsilon_{0\mathrm{w}} = 0.5$, $\chi_{\mathrm{w}} = 0.6$, $\nu = 1.0$, $\mu = 0.5$ and $\chi'_{\mathrm{w}} = 0.6$. ϕ_{wall} gives the minimum value with $e_{i,z} = 0$, therefore, the walls of the slit have a planar surface. However, there is no particular direction on the surface. Additionally, the wall described by Equation (5) is flat and has no structure fixed on the surface. Therefore, we can investigate confined uniaxial ellipsoids in the $NhP_{\|}T$ ensemble, which allows the fluctuation of the base area. There are several choices for the definition of the slit gap [18,25]. In our study, the exclusive volumes of a wall and a particle have been included in the definition. According to the definition, the slit gap is 6.0, z_{w} is set to 0

and $6.0 + 2\Delta z$. Δz is a constant and has a low quantity, which includes the effect of the exclusive volumes of a particle and a wall; the details have been reported in [31]. The spherical cutoff distance of 4.0 is applied to both potentials independent of the ellipsoid's orientation.

The results for this model are given in length, energy, mass, moment of inertia, time, pressure and temperature units of σ_0, ϵ_0, m, I, $\sqrt{m\sigma^2/\epsilon_0}$, $\sqrt{\epsilon_0/\sigma^3}$ and ϵ_0/k_B, respectively. m is the mass and I is the moment of inertia of a particle. The timestep was set to 0.005 over all the simulations.

2.3 Initial condition

The initial conditions are prepared as follows: first, the system equilibrated with $N = 1000$ is prepared at $T = 1.20$, 1.15, 1.10, 1.05 and 1.00. Next, these systems are duplicated in the x- and y-directions and the systems of $N = 9000$, 16,000, 64,000 and 100,000 are made. The system of $N = 169{,}000$ is also made at $T = 1.20$, 1.15 and 1.10. Finally, the noise of ± 0.001 is randomly added to momenta of all the particles. The simulations start from these configurations and the growth or decay of the ordered structure is investigated. $(N, T) = (100{,}000, 1.10)$, $(169{,}000, 1.10)$, $(100{,}000, 1.15)$, $(169{,}000, 1.15)$, $(100{,}000, 1.20)$ are investigated until the time of up to 10,000, the other conditions are simulated until the time of 5000.

2.4 Quantities output

In order to judge whether the particles in the quasi-2-dimensional system were fluid or solid, it was required to calculate the 1-dimensional number density profile (1DND) and 2-dimensional mean square displacement (2DMSD). The 1DND, $\rho_{1D}(z)$ reveals the translational order of the centres of mass of particles along z-axis [25,38]. The system was resolved into thin sheets parallel to the slit with the thickness of 0.1, and $\rho_{1D}(z_i)$ is calculated for every sheet:

$$\rho_{1D}(z_i) = \left\langle \frac{1}{V_i} \sum_{j \in C_{1D,i}} 1 \right\rangle, \tag{9}$$

where $C_{1D,i}$ is the ith sheet from the wall at $z = 0$, z_i represents the z-position of the ith sheet, and V_i is the volume of a sheet. The value of 0 is output near the walls because the repulsive force of the walls excludes particles. The 2DMSD, $M_{2D}(t)$, shows the mobility of particles along the x- and y-directions

$$M_{2D}(t) = \left\langle \frac{1}{N} \sum_{i=1}^{N} \{\boldsymbol{q}_{2D,i}(t) - \boldsymbol{q}_{2D,i}(0)\}^2 \right\rangle, \tag{10}$$

where $\boldsymbol{q}_{2D,i} = (x_i, y_i)$ is the 2-dimensional positional vector, whose two components are ones of the ith 3-dimensional positional vector, $\boldsymbol{q}_i$. To calculate $\rho_{1D}(z)$ and $M_{2D}(t)$, the additional simulations for the time of 100 were carried from the terminal time of monitoring. $M_{2D}(t)$ is defined between $0 \le t \le 4.0$. Moreover, the 2-dimensional self-diffusion coefficients (2DSDC), D_{2D}, were calculated from the time-derivatives of $M_{2D}(t)$ between $2.0 \le t \le 4.0$ [39].

We define the 1-dimensional order parameter (1DOP), P_{1D}, for the orientations of particles in the slit [25]. P_{1D} describes whether the uniaxial particles tend to be perpendicular or parallel to the z-axis:

$$P_{1D} = \left\langle \frac{1}{N} \sum_{i=1}^{N} \frac{3e_{i,z}^2 - 1}{2} \right\rangle. \tag{11}$$

When all particles are perpendicular to the z-axis, or parallel to the slit, $P_{1D} = -0.5$. When all particles are parallel to the z-axis or perpendicular to the slit, $P_{1D} = 1.0$. When all particles are orientationally random, $P_{1D} = 0$. P_{1D} is also calculated and monitored through all simulations.

The eigenvectors of the following 3×3, traceless matrix are related to the characteristic directions of the uniaxial particles:

$$\boldsymbol{Q}_{3D} = \left\langle \frac{1}{N} \sum_{i=1}^{N} \frac{3\boldsymbol{e}_i \otimes \boldsymbol{e}_i - \mathbf{1}}{2} \right\rangle, \qquad \boldsymbol{e}_i = (e_{i,x}, e_{i,y}, e_{i,z}), \tag{12}$$

where $\mathbf{1}$ is the unit matrix and the angle bracket denotes the average over time. Diagonalisation of the matrix yields three eigenvalues, $P_{3D,1}$, $P_{3D,2}$, $P_{3D,3}$, where $P_{3D,1} > P_{3D,2} > P_{3D,3}$. When $P_{3D,1} > 0$, $P_{3D,2} = P_{3D,3}$, particles exhibit globally uniaxial state. When $P_{3D,1} > 0$, $P_{3D,1} > P_{3D,2} > P_{3D,3}$, particles exhibit biaxial state [42,43]. Particularly, $P_{3D,1}$ is called 3-dimensional order parameter (3DOP) and has been also very commonly calculated in bulk nematic LCs [39–41]. In the case of the bulk Gay–Berne particles with parameters in the current report, $P_{3D,1} \le 0.1$ when particles exhibit the isotropic phase. Since the number of particles is finite, $P_{3D,1} = 0$ is not generally realised. $0.6 \le P_{3D,1} \le 0.7$ when particles exhibit a global nematic behaviour and $P_{3D,1} \ge 0.9$ when they are solid with a global uniaxiality.

The 2-dimensional azimuth histogram (2DAH), $f(\phi)$, explicitly shows the characteristic directions in the xy plane, where ϕ is the azimuth angle from the x-axis.

$$f(\phi) = \left\langle \frac{1}{N\Delta\phi} \sum_{i \in \{\phi < \phi_i < \phi + \Delta\phi\}} 1 \right\rangle, \tag{13}$$

where ϕ_i is the azimuth angle between the long axis of the ith particles and x-axis. It is sufficient that ϕ is defined between $-90°$ and $+90°$. When the orientations of the

particles are perfectly random, $f(\phi)$ is uniform and the value is constant, $1/180 \simeq 0.00556$.

We will observe that the weak local orientational order may propagate to a rather distant place at some temperature when uniaxial particles are confined in the flat, structureless slit. The analysis of this effect was carried out through a 2-dimensional mutual orientational correlation function (2DMOCF) [32]. First, $n_{2D}(r_{2D})$ is defined as the number of particles between $(r_{2D}, r_{2D} + \Delta r)$, where r_{2D} is the 2-dimensional distance in the xy plane. $n_{2D}(r_{2D})$ is then given by

$$n_{2D}(r_{2D}) = \left\langle \frac{1}{N_{\text{sample}}} \sum_{i=1}^{N_{\text{sample}}} \sum_{j \in \{j \neq i, C_{r_{2D}}\}} 1 \right\rangle, \tag{14}$$

where N_{sample} is the number of ith particles in one timestep, and $C_{r_{2D}}$ is the region between cylinders with the radius of r_{2D} and $r_{2D} + \Delta r$, that are parallel to the z-axis. Using $n_{2D}(r_{2D})$, 2DMOCF, $h_{2D}(r_{2D})$, is defined as

$$h_{2D}(r_{2D}) = \frac{1}{n_{2D}(r_{2D})} \left\langle \frac{1}{N_{\text{sample}}} \cdot \sum_{i=1}^{N_{\text{sample}}} \sum_{j \in \{j \neq i, C_{r_{2D}}\}} \left(2\cos^2 \theta_{ij} - 1\right) \right\rangle, \tag{15}$$

$$\cos^2 \theta_{ij} = (\boldsymbol{e}_i . \boldsymbol{e}_j)^2. \tag{16}$$

It should be noted that $h_{2D}(r_{2D})$ has a relation to the quasi-2-dimensional radius distribution function,

$$g_{2D}(r_{2D}) = \frac{1}{2\pi r \Delta r \bar{\rho}} n_{2D}(r_{2D}), \tag{17}$$

through the following equation:

$$h_{2D}(r_{2D}) = \frac{1}{2\pi r_{2D} \Delta r \bar{\rho} g_{2D}(r_{2D})} \times \left\langle \frac{1}{N_{\text{sample}}} \times \sum_{i=1}^{N_{\text{sample}}} \sum_{j \in \{j \neq i, C_{r_{2D}}\}} 2\cos^2 \theta_{ij} - 1 \right\rangle, \tag{18}$$

where $\bar{\rho} = N/V$. In other words, $h_{2D}(r_{2D})$ is normalised by $g_{2D}(r_{2D})$ and $h_{2D}(r_{2D})$ does not include the information of the structure of the centres of the mass of particles. Therefore, only local orientational correlation is calculated. In the Appendix, the result of the 3-dimensional mutual orientational correlation function (3DMOCF) in the 3-dimensional bulk system is reported to compare with 2DMOCF. 2DMOCF is calculated in the time of 100 from the terminal time.

3. Results and discussion

1DND, $\rho_{1D}(z)$ and 2DMSD, $M_{2D}(t)$, are shown in Figures 1 and 2 in order to examine the fluidity of centres of mass around the terminal time. Additionally, 2DSDC is listed in Table 2. All $\rho_{1D}(z)$ at a specific temperature appear the same; the profiles have six local maximums and five local minimums. These shapes lead to the fact that the centres of mass of particles tend to fabricate six layers in the slit with $h = 6.0$. According to $\rho_{1D}(z)$ in $1.20 \geq T \geq 1.05$ (Figure 1(a–d)), particles possess a fluidity in the z-direction,

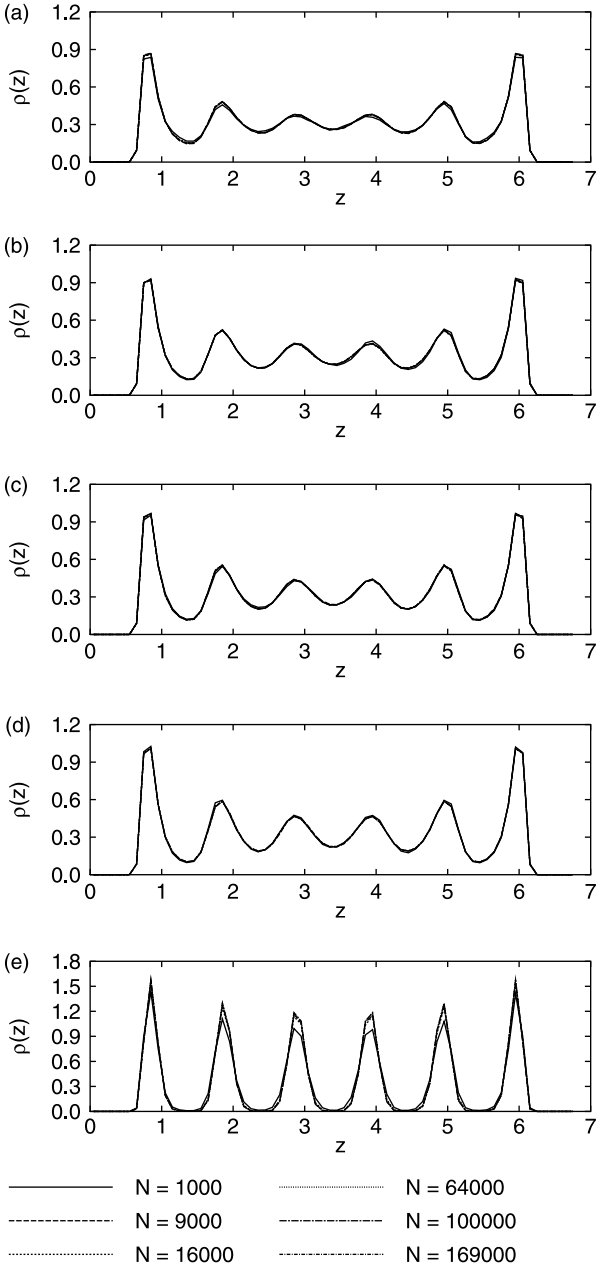

Figure 1. 1-dimensional number density profile (1DND), $\rho_{1D}(z)$. (a) $T = 1.20$, (b) $T = 1.15$, (c) $T = 1.10$, (d) $T = 1.05$ and (e) $T = 1.00$.

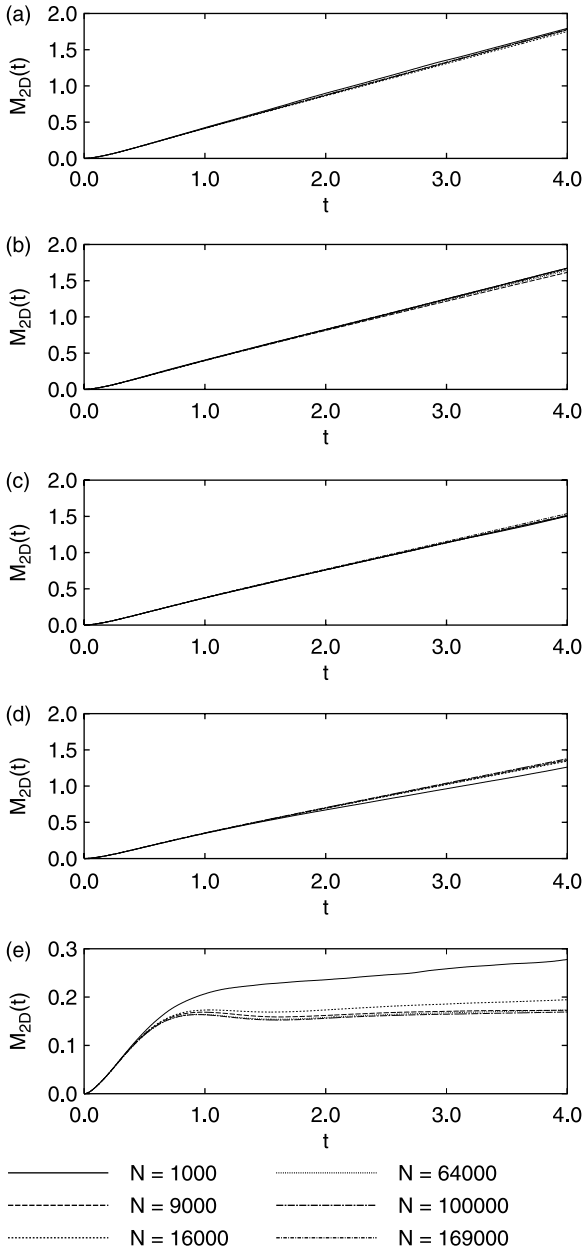

Figure 2. 2-dimensional mean square displacement (2DMSD), $M_{2D}(t)$. (a) $T = 1.20$, (b) $T = 1.15$, (c) $T = 1.10$, (d) $T = 1.05$ and (e) $T = 1.00$.

because values of local minimums are in the order of 0.1 and not regarded as small. This means a shift in particles between layers. In the case of the bulk system, particles are in the isotropic phase when $T \geq 1.15$. Particles in the slit, however, have some structure at such a temperature. We consider that the walls affect particles fabricating in some order. Upon a cooling of the system, the maximums of $\rho_{1D}(z)$ increase and the minimums decrease. This means that the fluid becomes more structurised. In $1.20 \geq T \geq 1.05$, all of $M_{2D}(t)$ are linear between the time of 2.0 and 4.0 (Figure 2(a–d)). This

Table 1. 2-dimensional self-diffusion coefficient (2DSDC), D_{2D}. 2DSDCs were calculated from the terminal time of simulation in time of 100.

T	N	L	D_{2D}
1.20	1000	23.1	0.0559
	9000	68.9	0.0539
	16,000	92.0	0.0555
	64,000	184.0	0.0563
	100,000	230.0	0.0565
	169,000	299.0	0.0566
1.15	1000	22.8	0.0533
	9000	68.3	0.0501
	16,000	91.1	0.0521
	64,000	182.2	0.0524
	100,000	227.7	0.0527
	169,000	296.2	0.0527
1.10	1000	22.6	0.0459
	9000	67.8	0.0465
	16,000	90.5	0.0466
	64,000	180.8	0.0465
	100,000	226.0	0.0470
	169,000	293.9	0.0479
1.05	1000	22.4	0.0366
	9000	67.4	0.0415
	16,000	89.8	0.0407
	64,000	179.7	0.0411
	100,000	224.6	0.0421
1.00	1000	22.0	0.0026
	9000	65.6	0.0005
	16,000	87.4	0.0016
	64,000	174.6	0.0009
	100,000	218.3	0.0059

Note: As the reference, the length of the edge of the area, L, is also listed, which was averaged from the time of 3500 to the terminal time.

suggests that particles possess a fluidity not only in the z but also in the x- and y-directions. The value of $M_{2D}(t = 4.0)$ decreases and the diffusivity of particles also decreases when the temperature decreases. 2DSDC actually decreases when the temperature decreases (Table 1). As a result, the centres of mass of particles are in the fluid phase at $T \geq 1.05$. In the case of $T = 1.00$, on the other hand, the values of the minimums of $\rho_{1D}(z)$ are in the order of 0.01 (Figure 1(e)). This means that particles hardly move from one layer to another. Figure 2(e) shows that $M_{2D}(t)$ hardly increases from $t \geq 2.0$. D_{2D} is smaller by one figure than the ones at the other higher temperatures (Table 1). Thus, the centres of mass hardly diffuse in the x-, y- and z-directions and they are finally in the solid phase for all Ns at $T = 1.00$. In this report, the numerical accuracy of $M_{2D}(t)$ and D_{2D} is not strictly discussed because the sampling time is short. However, the sampling time of 100 is not regarded to be poor in order to just judge the fluidity of the centres of mass.

It has been found that Gay–Berne particles in the slit at $P_{\|} = 4.5$ are in the fluid phase when $T \geq 1.05$, and in the solid phase when $T = 1.00$. In the bulk system, the isotropic–nematic phase transition temperature is between

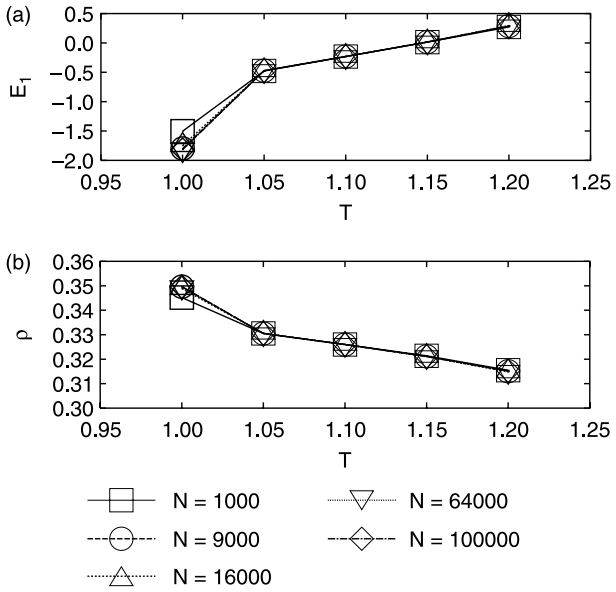

Figure 3. (a) One-particle energy, E_1 and (b) number density, ρ, as a function of temperature, T.

$T = 1.15$ and 1.10 at $P_{\parallel} = 4.5$; it is a first order phase transition. However, the total energy of the physical system and the number density do not jump between $T = 1.15$ and 1.10 when particles are confined in the slit. The total energy of the physical system per particle, $E_1 = E/N$, is shown in Figure 3(a), and the number density, $\rho = N/V$, is shown in Figure 3(b). E_1 is described as follows:

$$E_1 = \frac{E}{N}, \tag{19}$$

$$E = \sum_{i=1}^{N} \frac{\boldsymbol{p}_i}{2m} + \frac{I\boldsymbol{u}_i}{2} + \sum_{i=1}^{N} \sum_{j>i} \phi_{\mathrm{GB}}(\boldsymbol{r}_{ij}, \boldsymbol{e}_i, \boldsymbol{e}_j) + \sum_{i=1}^{N} \phi_{\mathrm{wall}}(z_i, \boldsymbol{e}_i; 0) + \sum_{i=1}^{N} \phi_{\mathrm{wall}}(z_i, \boldsymbol{e}_i; h + 2\Delta z), \tag{20}$$

where $\boldsymbol{p}_i$ is the momentum and $\boldsymbol{u}_i$ is the time derivative of the orientation vector of ith particle. In the pseudo-2-dimensional system, both E_1 and ρ seem to continuously vary. It was found that the particles in the thin slit do not exhibit the first order isotropic–nematic phase transition; therefore they show orientational properties different from the ones in the bulk system.

We have examined the order of the centres of mass of particles in the final phase. The following part describes the orientational state of the particles. In Table 2, the averaged values of 1DOP, 3DOP and the other two eigenvalues of (12) are listed from $t = 3500$ to the terminal time; as seen afterwards, the start time of 3500 is sufficient to average quantities because the initial condition of particles relaxes by $t = 3500$. First, 1DOP, P_{1D}, was a negative value between -0.44 and -0.29 from $t = 3500$ over all conditions and the deviation was relatively small. This suggests that the particles tend to be parallel to the slit. Particles are in the isotropic phase and orientationally random in the bulk system at $T = 1.20$ and 1.15, however, they are strongly constrained in the xy plane. Next, 3DOP, $P_{3D,1}$, decreased when the number of particles or cell size increased. Rull et al. have observed such dependence with the film of the Gay–Berne particles on the smooth surface. Then, $P_{3D,2}$ and $P_{3D,3}$ did not coincide with each other in the fluid conditions and the difference between them increased upon a increasing the cell size; $P_{3D,2}$ increased up to a positive value in the system with over 100,000 particles at $1.20 \geq T \geq 1.10$ and 64,000 particles at $T = 1.05$. The biaxiality of particles is suggested at such conditions.

Figure 4 shows the monitor of 3DOP, $P_{3D,1}$. When particles are confined in the slit, $P_{3D,1}$ outputs a non-zero value even at the temperature corresponding to the isotropic phase in the bulk system. However, we should carefully investigate the N dependence on the orientational property of the confined particles. When $N \leq 64{,}000$ at $T = 1.20$ (Figure 4(a)), $P_{3D,1}$ oscillates between 0.2 and 0.6 (Table 2). Such values are not observed when the particles are in the 3-dimensional bulk system (see Appendix). When $N \geq 100{,}000$, $P_{3D,1}$ decays to 0.2. It is found that $P_{3D,1}$ may not decrease to under 0.2 when the Gay–Berne particles are confined in the slit. We consider that one of the causes is the strong confinement. When the orientations of the particles are 3-dimensionally random, $P_{3D,1}$ is nearly equal to 0 and no characteristic direction is in the system. Particles confined in the slit, however, tend to be parallel to the xy plane and their orientations are not absolutely random, as is mentioned P_{1D}. As a result, $P_{3D,1}$, which is a quantity averaged over the x-, y- and z-directions, does not decrease under a value of 0.2. The point is that the system of $N \geq 100{,}000$ or $L \geq 230.0$ should be regarded as sufficient so that N or L dependence is excluded. When $T = 1.15$, particles in the bulk system are in the isotropic phase. Particles confined in the slit, however, possess orientational properties different from ones of the bulk system (Figure 4(b)). When $N \leq 16{,}000$, $P_{3D,1}$ is between 0.5 and 0.6; the range of $P_{3D,1}$ is not observed in the bulk system. This is a situation similar to the case of $T = 1.20$. On the other hand, $P_{3D,1}$ gradually decreases by $t = 5000$ in the case of $N = 64{,}000$. Finally, $P_{3D,1}$ decays to 0.2 in $3000 \leq t \leq 4000$, fluctuates around $P_{3D,1} = 0.3$ with the deviation about 0.06 when $N \geq 100{,}000$ or $L \geq 227.7$. The fluctuation has a rather long period and does not converge in $t = 10{,}000$. The magnitude of $P_{3D,1}$ for $N = 100{,}000$ appears equal in $t \geq 3{,}500$, compared with the one of $N = 169{,}000$. This slow fluctuation of the orientational order might be a property of the uniaxial particles confined in the flat, structureless slit. When

Table 2. 1-dimensional order parameter (1DOP), P_{1D}, 3-dimensional order parameter (3DOP), $\pm P_{3D,1}$, and the other two eigenvalues of (12), $P_{3D,2}$; $P_{3D,3}$.

T	N	L	P_{1D}	$P_{3D,1}$	$P_{3D,2}$	$P_{3D,3}$
1.20	1000	23.1	−0.298 ± 0.015	0.465 ± 0.092	−0.158 ± 0.079	−0.307 ± 0.016
	9000	68.9	−0.295 ± 0.004	0.370 ± 0.034	−0.075 ± 0.033	−0.295 ± 0.003
	16,000	92.0	−0.288 ± 0.003	0.286 ± 0.029	0.002 ± 0.029	−0.288 ± 0.005
	64,000	184.0	−0.295 ± 0.002	0.253 ± 0.027	0.041 ± 0.026	−0.293 ± 0.002
	100,000	230.0	−0.296 ± 0.002	0.226 ± 0.030	0.071 ± 0.030	−0.297 ± 0.003
	169,000	299.0	−0.296 ± 0.001	0.198 ± 0.016	0.099 ± 0.016	−0.297 ± 0.002
1.15	1000	22.8	−0.337 ± 0.008	0.603 ± 0.027	−0.262 ± 0.019	−0.342 ± 0.009
	9000	68.3	−0.337 ± 0.002	0.577 ± 0.006	−0.238 ± 0.005	−0.339 ± 0.004
	16,000	91.1	−0.337 ± 0.002	0.563 ± 0.016	−0.224 ± 0.015	−0.338 ± 0.001
	64,000	182.2	−0.337 ± 0.001	0.473 ± 0.009	−0.136 ± 0.009	−0.337 ± 0.001
	100,000	227.7	−0.338 ± 0.001	0.318 ± 0.071	0.020 ± 0.071	−0.337 ± 0.001
	169,000	296.2	−0.339 ± 0.001	0.286 ± 0.049	0.053 ± 0.049	−0.339 ± 0.001
1.10	1000	22.6	−0.361 ± 0.006	0.668 ± 0.011	−0.303 ± 0.009	−0.366 ± 0.005
	9000	67.8	−0.361 ± 0.002	0.645 ± 0.010	−0.285 ± 0.008	−0.360 ± 0.004
	16,000	90.5	−0.361 ± 0.001	0.642 ± 0.008	−0.280 ± 0.008	−0.362 ± 0.001
	64,000	180.8	−0.362 ± 0.001	0.600 ± 0.006	−0.238 ± 0.006	−0.362 ± 0.001
	100,000	226.0	−0.361 ± 0.001	0.314 ± 0.054	0.047 ± 0.054	−0.361 ± 0.001
	169,000	293.9	−0.361 ± 0.001	0.285 ± 0.046	0.076 ± 0.046	−0.361 ± 0.001
1.05	1000	22.4	−0.378 ± 0.003	0.715 ± 0.015	−0.335 ± 0.012	−0.380 ± 0.006
	9000	67.4	−0.378 ± 0.002	0.697 ± 0.004	−0.318 ± 0.004	−0.379 ± 0.001
	16,000	89.8	−0.378 ± 0.001	0.685 ± 0.009	−0.307 ± 0.009	−0.379 ± 0.001
	64,000	179.7	−0.377 ± 0.001	0.234 ± 0.018	0.143 ± 0.018	−0.376 ± 0.001
	100,000	224.6	−0.378 ± 0.001	0.219 ± 0.010	0.159 ± 0.010	−0.377 ± 0.001
1.00	1000	22.0	−0.427 ± 0.001	0.875 ± 0.007	−0.434 ± 0.005	−0.441 ± 0.003
	9000	65.6	−0.436 ± 0.000	0.917 ± 0.001	−0.455 ± 0.001	−0.462 ± 0.000
	16,000	87.4	−0.435 ± 0.000	0.910 ± 0.003	−0.451 ± 0.003	−0.459 ± 0.000
	64,000	174.6	−0.437 ± 0.000	0.919 ± 0.000	−0.456 ± 0.000	−0.463 ± 0.000
	100,000	218.3	−0.437 ± 0.000	0.920 ± 0.000	−0.456 ± 0.000	−0.464 ± 0.000

Note: Quantities were averaged from the time of 3500 to the terminal time.

$T = 1.10$, particles exhibit a nematic behaviour in the 3-dimensional bulk system. On the other hand, particles in the slit do not equilibrate to the nematic phase, that is, globally uniaxial state(Figure 4(c)). In the case of $T = 1.10$, $P_{3D,1}$ remains around 0.6 through the simulation when $N \leq 64{,}000$ and this result suggests that particles exhibit a nematic behaviour. However, the uniaxiality gradually decreases, and decays to 0.2 for $N \geq 100{,}000$ or $L \geq 226.0$. Similar to the case of $T = 1.15$ and $N \geq 100{,}000$, $P_{3D,1}$ fluctuates with a very long period and does not converge in $t = 10{,}000$. The average of $P_{3D,1}$ is 0.3 and the deviation is about 0.06 for $t \geq 3500$. In the case of $T = 1.05$(Figure 4(d)), $P_{3D,1}$ remains around 0.7 through the simulation when $N \leq 16{,}000$ and the result suggests that particles exhibit a nematic behaviour. However, the lower value of $P_{3D,1}$ is output when $N \geq 64{,}000$ or $L \geq 179.7$; $P_{3D,1}$ decays to 0.2 in $1000 \leq t \leq 3000$. It is suggested that the system does not possess the global uniaxiality. When $T = 1.00$, particles are in the solid phase in the 3-dimensional bulk system. We have confirmed that centres of mass of particles in the slit are in the solid phase. From Figure 4(e), we can observe that high orientational order is also kept over all the number of particles. Figure 4(e), however, also suggests that the system of $N = 1000$ is different from other systems in the detailed orientational order. The terminal value of $P_{3D,1}$ in $N = 1000$ is 0.86. On the other hand, $P_{3D,1}$ in $N \geq 9000$ grows; the terminal value is 0.91 in $N = 64{,}000$ and 100,000. It is found that all systems in $T = 1.00$ are stable in uniaxial solid. We consider, however, 9000 particles or more should be prepared when Gay–Berne particles in the solid phase are investigated in an infinitely wide slit.

Figures 5(a) and (b) summarise the $P_{3D,1}$ averaged from the time of 3500 to the terminal time and reveal the N and L dependence of the uniaxiality of the Gay–Berne particles in the flat, structureless slit, respectively. For all five temperatures, the orientational order depends on the number of particles. It is found that the dependence on N or L is excluded for the system of $N \geq 100{,}000$ or $L \geq 220$ at $T \geq 1.10$. When $T = 1.05$, $N \geq 64{,}000$ or $L \geq 180$ gives the different orientational order from the one with the smaller N or L.

We have found that the fluid of 100,000 particles or more, in other words, the fluid in the slit whose base has edges of 220 or more, loses its global uniaxiality. Actually, Table 2 has already suggested the biaxiality at such conditions. The orientational state and characterinsic

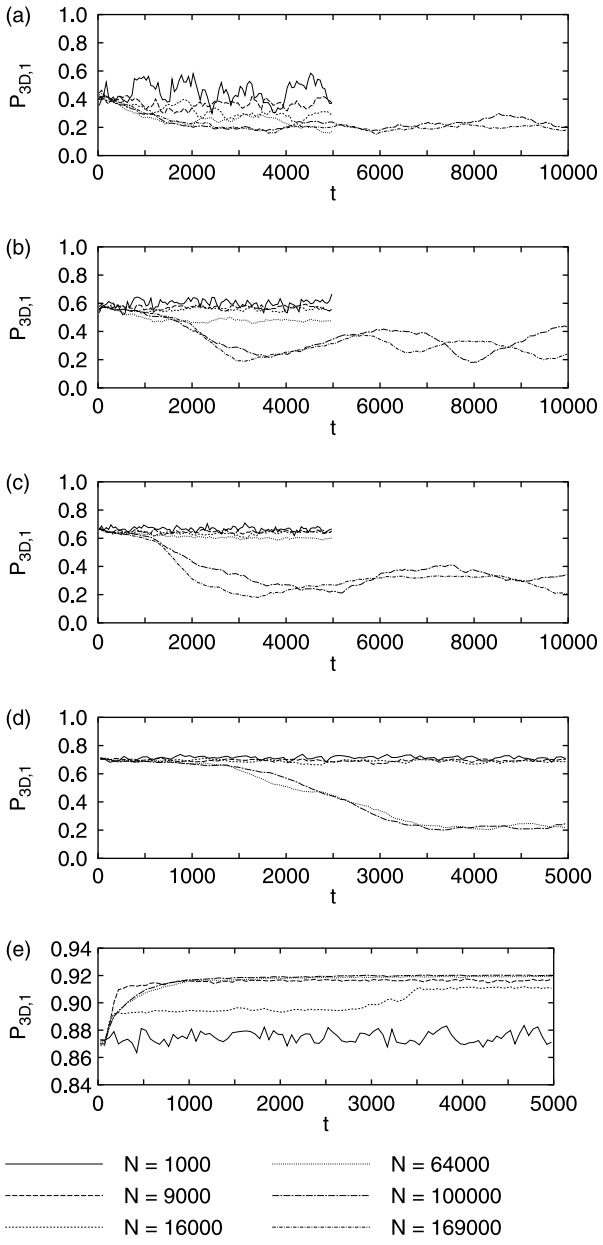

Figure 4. Monitoring of 3-dimensional order parameter (3DOP), $P_{3D,1}$. (a) $T = 1.20$, (b) $T = 1.15$, (c) $T = 1.10$, (d) $T = 1.05$ and (e) $T = 1.00$. 3DOPs for $N = 169{,}000$ are shown in $T = 1.20$, 1.15 and 1.10.

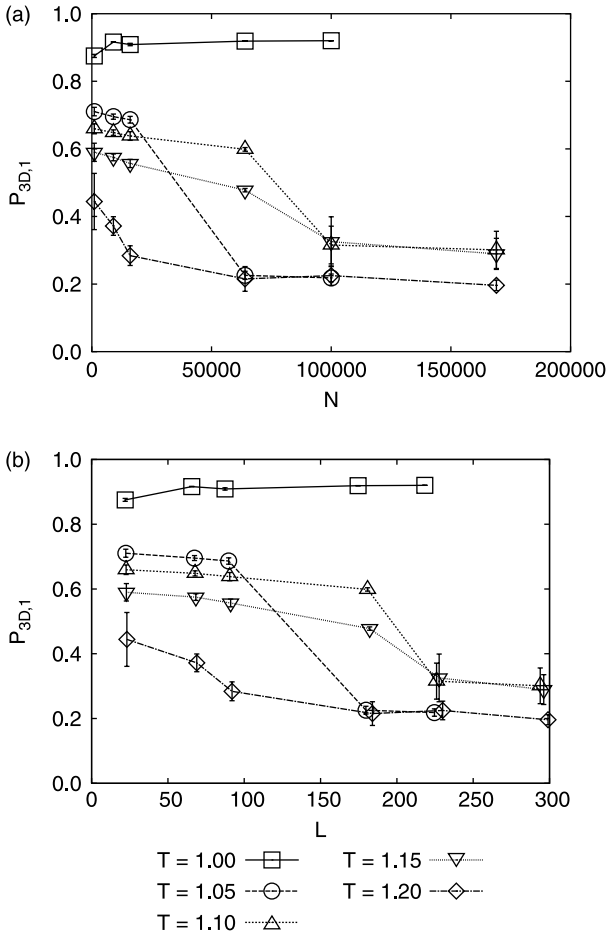

Figure 5. N and L-dependence of the uniaxiality of Gay–Berne nematogen in the flat, structureless slit, $P_{3D,1}$. (a) N-dependence and (b) L-dependence. $P_{3D,1}$ is averaged from $t = 3500$ to the terminal time.

directions in the xy plane of $N = 100{,}000$ are studied in detail by 2DAH, $f(\phi)$ (Figure 6). As a reference, the histograms around $t = 500$ are shown at all temperatures. They have one maximum at an azimuth. Around the azimuth perpendicular to it, one minimum is observed; the value of the minimum is one-tenth that of the maximum one. Thus, the system possesses a global uniaxiality in the xy plane during the initial phase of the simulation. It is very natural because the system with over 1000 particles was made from the system of 1000 particles. The orientational state varies with time. At $T = 1.20$ (Figure 6(a)), $f(\phi)$ is broadly around $t = 10{,}000$. It is suggested that the system loses its uniaxiality. At $T = 1.15$ (Figure 6(b)), $f(\phi)$ around $t = 500$, 8000 and 10,000 are depicted. $f(\phi)$ around $t = 8000$ has two maximums at $\phi = 55$ and 131 and the one around $t = 10{,}000$ has one maximum at $\phi = 83$. Thus the uniaxiality around $t = 500$ decays, the system exhibits both the biaxial state around $t = 8000$, and the uniaxial state around $t = 10{,}000$. Figure 4(b) has shown that $P_{3D,1}$ fluctuates, the value is about 0.2 around $t = 5000$ and 0.4 around $t = 10{,}000$. Therefore, it is suggested that the system of $N = 100{,}000$ oscillates between the biaxial state corresponding to the small $P_{3D,1}$ and the uniaxial state corresponding to the large $P_{3D,1}$. At $T = 1.10$ (Figure 6(c)), $f(\phi)$ around $t = 500$, 5000 and 10,000 is depicted. $f(\phi)$ around $t = 5000$ has two maximums at $\phi = 90$ and 179. $f(\phi)$ around $t = 10{,}000$ has one high maximum at $\phi = 59$ and one rather smaller maximum at $\phi = 131$. The oscillation between the two

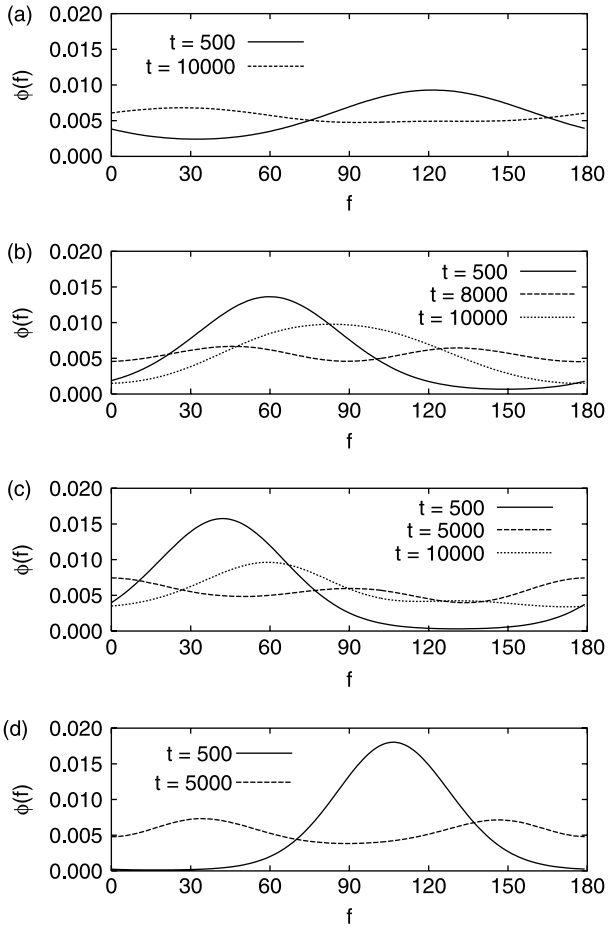

Figure 6. 2-dimensional azimuth histogram (2DAH). (a) $T = 1.20$, (b) $T = 1.15$, (c) $T = 1.10$ and (d) $T = 1.05$.

orientational states is also observed at $T = 1.10$ with $N \geq 100{,}000$. When $T = 1.05$, no oscillation is observed; $f(\phi)$ has two maximums from $t = 3500$. This suggests that the system has possessed the biaxiality from 3500.

We have reviewed the possibility that the systems of $N \geq 100{,}000$ possess a biaxiality. 2DAH shows two maximums. However, the difference between the value of maximum and the uniform value, 0.00556, is small, and some people might identify weak maximums as just deviations in the histograms. However, snapshots actually show that particles distribute with characteristic directions (Figure 7). For the concise recognition of the biaxiality in the *xy* plane, the figures do not show all of the particles. First, one orientational vector, e_i, is randomly chosen, The *i*th particles and the others that satisfy

$$|\boldsymbol{e}_i.\boldsymbol{e}_j| \geq \frac{\sqrt{3}}{2} \tag{21}$$

are then depicted. Of course, the slit is filled by particles and no bubble is in the slit because the system is equilibrated through the $NhP_{\parallel}T$ ensemble. In $T = 1.20$ (Figure 7(a)), particles satisfying Equation (21) widely distribute and no clear boundaries of domains might appear. When $T = 1.15$, the distribution of particles is significantly biased. Figure 7(b) is taken at $t = 8000$ in $T = 1.15$. Particles satisfying Equation (21) gather and the domain is presented along the *y*-direction from the centre of the *xy* plane. This snapshot directly shows the biaxiality of particles in the flat, structureless slit because particles, which tend to be perpendicular to the *i*th particles, exist beside the domain shown and they form other domains. On the other hand, Figure 7(c) at $t = 10{,}000$ at $T = 1.15$ shows a uniaxiality; particles satisfying Equation (21) distribute over the slit. We have also confirmed such an orientational domain structure at $T = 1.10$. Figure 5 has shown no clear discontinuous shift, which is related to the first order isotropic–nematic phase transition, however, a global transition might occur near $T = 1.15$ and 1.10. Finally, the clear domain structure is observed and the system is in the biaxial state at $T = 1.05$ (Figure 7(d)). The figure suggests that there are two stable nematic domains.

2DMOCF, $h_{2D}(r_{2D})$, is depicted in Figure 8 in order to investigate the orientational order which can propagate over the system. 3DMOCF, $h(r)$ as the reference is shown in Figure 9 in the Appendix. When $T = 1.20$ or 1.15, the behaviour of the tail of $h_{2D}(r_{2D})$ is different from the result of the bulk isotropic system of $h_{2D}(r_{2D})$; $h_{2D}(r_{2D})$ gradually decreases with $r_{2D} > 1$ (Figure 8(a) and (b)). Such a gradual decay is not observed in the bulk isotropic 3DMOCF (see Appendix). When the tail of $h_{2D}(r_{2D})$ is compared with the one of 3DMOCF, we can understand that the $P_{3D,1}$ of $N \leq 64{,}000$ at $T = 1.20$ and 1.15 has taken an ambiguous value of $0.2 \leq P_{3D,1} \leq 0.4$. 3DMOCF converges well to 0 by $r \simeq 10.0$ when the system exhibits an isotropic phase, and it converges to 0.35 when the system exhibits a nematic behaviour. On the other hand, when particles are confined in the slit at $T = 1.20$ and 1.15, the weak spacial orientational correlation is cut off before the convergence. As a result, the weak local order remains by the periodic boundary condition, and causes the ambiguous values of $P_{3D,1}$ of particles in the slit. When $N \geq 100{,}000$ or $L \geq 227.7$ at $T = 1.20$ and 1.15, $h_{2D}(r_{2D})$ gradually decays, and the terminal value is around 0.1. It is found that the N or L dependence of $P_{3D,1}$ can be excluded when $h_{2D}(r_{2D})$ decays to about 0.1. Rull et al. also observed the weak orientational correlation of particles forming a thin film, which cannot be excluded until a large number of particles is prepared [32]. Figure 8(c) shows $h_{2D}(r_{2D})$ when $T = 1.10$. The terminal values of $h_{2D}(r_{2D})$ are over 0.4 when $N \leq 64{,}000$; it is suggested that particles in the slit exhibit a nematic behaviour. Actually, a $P_{3D,1}$ of 0.6 or more has been output. We consider that the spacial orientational correlation is cut off before a sufficient convergence and $P_{3D,1}$ for the nematic phase is output when the system is small. On the other hand, $h_{2D}(r_{2D})$ of $N \geq 100{,}000$ then gradually decays; the uniaxiality does

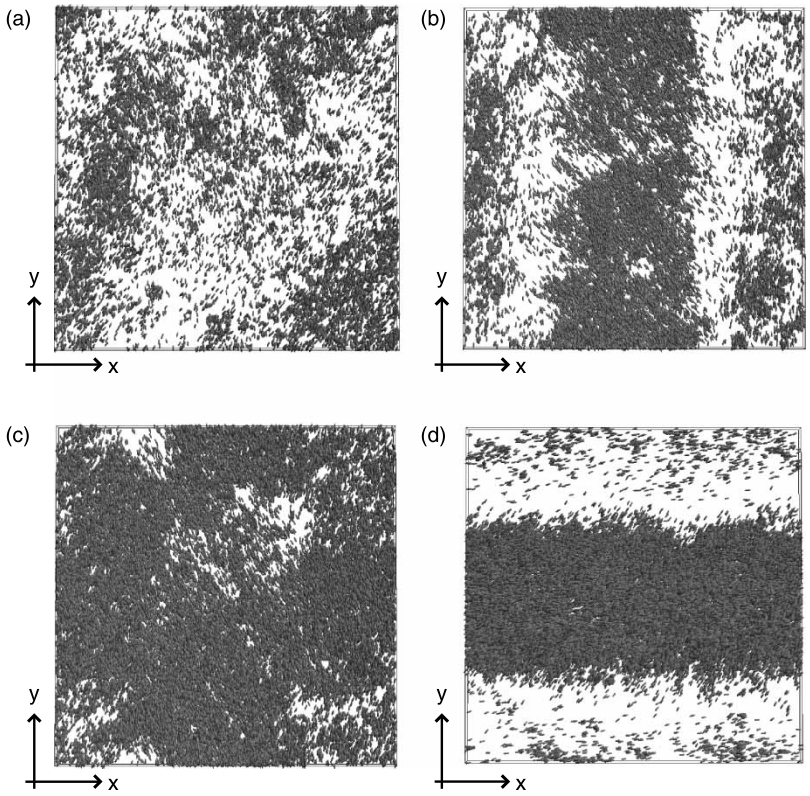

Figure 7. Snapshots with 100,000 particles. Periodic boundary condition is imposed in the x and y direction. (a) $T = 1.20$ at $t = 10{,}000$, $\boldsymbol{e}_i = (-0.20, -0.95, -0.26)$; (b) $T = 1.15$ at $t = 8000$, $\boldsymbol{e}_i = (-0.03, 0.99, 0.00)$; (c) $T = 1.15$ at $t = 10{,}000$, $\boldsymbol{e}_i = (0.24, -0.97, -0.07)$; (d) $T = 1.05$ at $t = 10{,}000$, $\boldsymbol{e}_i = (0.83, 0.56, -0.00)$.

not globally reach. As shown in Figures 7(b) and (c), the orientationally ordered domain is created and annihilated at $T = 1.15$ and 1.10. $h_{2D}(r_{2D})$, therefore, does not show the global uniaxiality. As in the case of $T = 1.20$ and 1.15, the system of $L \geq 226$ is preferred when $T = 1.10$. The shape of $h_{2D}(r_{2D})$ also depends on the number of particles at $T = 1.05$. When $N \leq 16{,}000$, the terminal values of $h_{2D}(r_{2D})$ are over 0.45, which is the same order of the ones in the bulk nematic phase. Since $P_{3D,1}$ is over 0.6, we want to determine that the system possesses a global uniaxiality, that is, a nematic order. However, the system with $N = 64{,}000$ or more realises several nematic domains; the corresponding L is 179.7. The point is that the different reason causes the N or L dependence of $P_{3D,1}$ at the temperature is 1.05. We consider that the clear appearance of the domain structure is the main cause of the dependence of 3DOP on the length of the edge of the area at the temperature of 1.05, rather than the weak orientational correlation. It should be noted that the shape of $h_{2D}(r_{2D})$ of the confined particles is not just cut off depending on N or L, but the shape itself transforms at $T = 1.10$ and 1.05. It is expected that the relation of the number of particles and the transformation of the shape of $h_{2D}(r_{2D})$ will be further investigated. When $T = 1.00$, $h_{2D}(r_{2D})$ hardly decays; the long-range orientational order covers particles and the particles in the slit are stable in the solid phase when $(P_{\|}, T) = (4.5, 1.00)$. Only the system of $N = 1000$ appears to have a terminal value under 0.8, which is regarded as the boundary value of the solid phase in the bulk system. It is found that the system with $N > 1000$ is preferred as mentioned for $P_{3D,1}$. The fact that the globally uniaxial solid is observed is natural because the system with $N > 1000$ has been duplicated from the system of $N = 1000$. We have reviewed, however, that 64,000 or more particles in the slit possess the domain structure when $T = 1.05$. When the particles at $T = 1.05$ are cooled into $T = 1.00$, they can be coagulated forming domains. In such a case, $h_{2D}(r_{2D})$ decays.

We have discussed the orientational order of uniaxial, prolate Gay–Berne particles in the flat, structureless slit. It should be noticed that the particles possess the weak orientational correlation even at the temperatures which correspond to the isotropic phase in the bulk system: 1.20 and 1.15. The fact that the weak correlation is cut off before the convergence causes the dependence of 3DOP on the length of the edge of the base. We believe that the causes of the weak correlation are not only that the particles tend to be parallel to the slit, but that the weak correlation also exists in the plane parallel to the slit. Figures 7(b) and (c) support our consideration; the

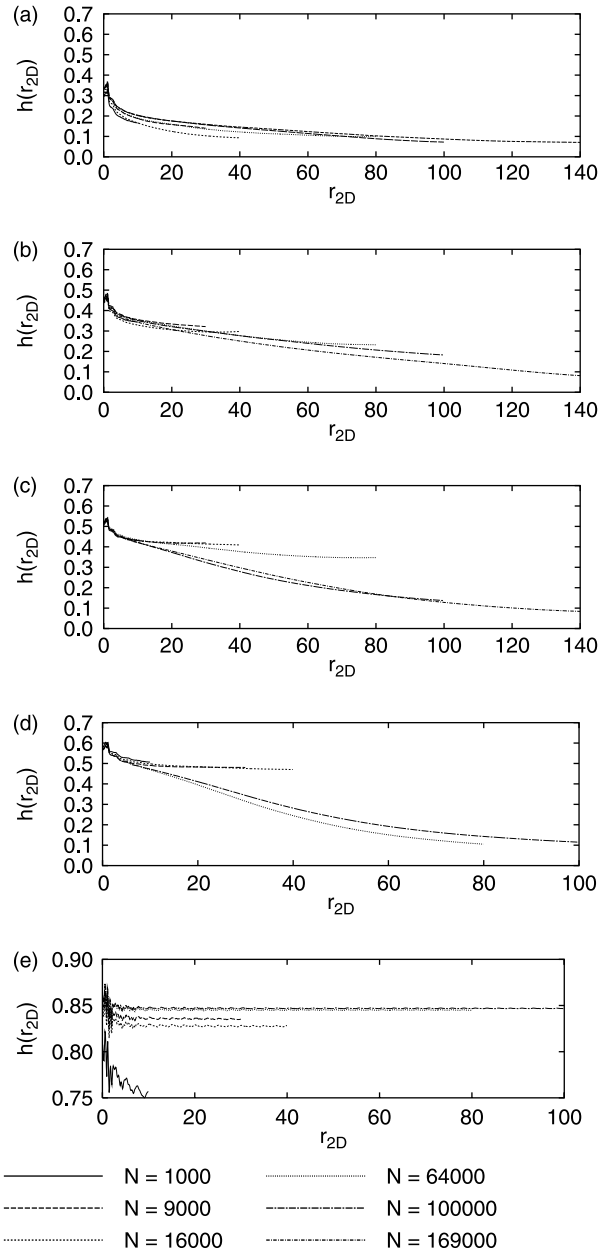

Figure 8. 2-dimensional mutual orientational correlation function (2DMOCF), $h(r_{2D})$. (a) $T = 1.20$, (b) $T = 1.15$, (c) $T = 1.10$, (d) $T = 1.05$ and (e) $T = 1.00$. 2DMOCFs for $N = 169{,}000$ are shown in $T = 1.20$, 1.15 and 1.10.

orientational correlation exists, but it is so weak that the domain structure is not maintained. We propose that the threshold of the number of particles is 100,000 so that the spacial correlation decays well when the Gay–Berne particles with the current potential parameters are confined in the slit with the slit gap of 6.0. Converting the number of particles into the length of the edge of the base, we can estimate 220 as the threshold of the length. When the value smaller than the threshold is applied, 2DMOCF is cut off before the convergence. This fact gives the critical misleading to the result of the simulation; the 3DOP depends on the cell length. When the temperature is 1.05, on the other hand, the clear appearance of the several domains is the main cause of the behaviour of the 2DMOCF and the dependence of 3DOP on the length of the edge of the area at the temperature of 1.05. The threshold of the length of the edge is 180, smaller than the one at the higher temperatures. When the length of the edge is smaller than the threshold, the global uniaxiality exists over the system. At this point, only one domain exists. However, several domains exist in the system, whose length of the edge is over the threshold, and 3DOP decreases. When one wants to investigate the particles in only one nematic domain at the temperature of 1.05, the simulation cell with the cell length smaller than the threshold of 180 can be prepared. However, when the particles in the slit are widely investigated at several thermodynamic conditions, considered the weak orientational correlation at the higher temperatures, the value of 220 as the length of the edge of the base is preferred.

4. Conclusion

We have carried out the constant pressure, temperature and slit gap classical molecular dynamics simulation so as to investigate the uniaxial prolate Gay–Berne particles confined in the flat, structureless slit. The fluidity and orientational structure were measured at five temperatures; the slit gap and pressure parallel to the slit are set 6.0 and 4.5, respectively.

The first order isotropic–nematic phase transition is not observed, even in the temperature range that covers both two phases in the bulk system. The orientational state of the particles in the slit depends on the number of particles or the length of the edge of the base. We proposed 220 as the threshold of the length of the edge. When the value over the threshold is used, the cell size dependence is excluded and the ambiguous results not observed. At this time, the local orientational order of the fluid particles gradually grows when the system is cooled. The particles exhibit the transitional behaviour of the creation and annihilation of the uniaxial domains. Several nematic domains are then clearly formed. If the system is further cooled, several nematic domains will be coagulated and the solid will be formed.

It is found that the Gay–Berne particles in the flat, structureless slit may not realise the globally uniaxial phase. Of course, particles are confined in the slit with some structure or roughness; therefore, some orders corresponding to the structure of the slit must be realised. When the slit has one characteristic direction, the global uniaxiality may be realised in the thin slit. The slit gap is then increased so that the region regarded as the bulk appears, thus it is possible that the globally uniaxial phase become stable. Finally, we should remember that the slit

gap is fixed to 6.0, that is, an integer. When an integer slit gap is applied, it is commensurate for particles with the short axis of 1.0; they are not disturbed and align parallel to the slit. For example, the slit gap equals a half-integer, and the particles cannot be equilibrated into the solid phase to a rather low temperature. The slit gap is a significant parameter in the case of confined particles, as is mentioned by Barmes and Cleaver [44] We are now investigating the phase transition of the uniaxial prolate Gay–Berne particles in the slit as a function of the slit gap.

Acknowledgements

We acknowledge Prof. M.P. Allen, Prof. P.M. Rodger and Dr. D. Cheung (University of Warwick) for their helpful discussions. This study was supported by a Grant-in-Aid for the 21st COE program at Keio University for 'System Design: Paradigm Shift from Intelligence to Life'. This research was partially supported by the Core Research for Evolution Science and Technology (CREST) of the Japan Science and Technology Corporation (JST).

References

[1] C. Tschierske, *Micro-segregation, molecular shape and molecular topology-partners for the design of liquid crystalline materials with complex mesophase morphologies*, J. Mater. Chem. 11 (2001), p. 2647.
[2] L.J. Ellison, D.J. Michel, F. Barmes, and D.J. Cleaver, *Entropy-driven formation of the gyroid cubic phase*, Phys. Rev. Lett. 97 (2006), p. 237801.
[3] C. Pujolle-Robic and L. Noirez, *Observation of shear-induced nematic–isotropic transition in side-chain liquid crystal polymers*, Nature 409 (2001), p. 167.
[4] G. Ungar, Y. Liu, X. Zeng, V. Percec, and W.D. Cho, *Giant supramolecular liquid crystal lattice*, Science 299 (2003), p. 1208.
[5] B.K. Cho, A. Jain, S.M. Gruner, and U. Wiesner, *Mesophase structure-mechanical and ionic transport correlations in extended amphiphilic dendrons*, Science 305 (2004), p. 1598.
[6] X. Zeng, G. Ungar, Y. Liu, V. Percec, A.E. Dulcey, and J.K. Hobbs, *Supramolecular dendritic liquid quasicrystals*, Nature 428 (2004), p. 157.
[7] E. de Miguel and E. Martín del Río, *Computer simulation of nematic reentrance in a simple molecular model*, Phys. Rev. Lett. 95 (2005), p. 217802.
[8] J.H. Kim, M. Yoneya, and H. Yokoyama, *Tristable nematic liquid–crystal device using micropatterned surface alignment*, Nature 420 (2002), p. 159.
[9] D. Andrienko, M. Tasinkevych, P. Patrício, M.P. Allen, and M.M.T. da Gama, *Forces between elongated particles in a nematic colloid*, Phys. Rev. E 68 (2003), p. 51702.
[10] M.C. Choi, T. Pfohl, Z. Wen, Y. Li, M.W. Kim, J.N. Israelachvili, and C.R. Safinya, *Ordered patterns of liquid crystal toroidal defects by microchannel confinement*, Proc. Natl. Acad. Sci. 101 (2004), p. 17340.
[11] B. Coasne, J. Czwartos, K.E. Gubbins, F.R. Hung, and M. Sliwinska-Bartokowiak, *Freezing of mixtures confined in a slit nanopore*, Adsorption 11 (2005), p. 301.
[12] L.D. Gelb and K.E. Gubbins, *Kinetics of liquid–liquid phase separation of a binary mixture in cylindrical pores*, Phys. Rev. E 55 (1997), p. 1290.
[13] B. Coasne, S.K. Jain, and K.E. Gubbins, *Freezing of fluids confined in a disordered nanoporous structure*, Phys. Rev. Lett. 97 (2006), p. 105702.
[14] R. Radhakrishnan and K.E. Gubbins, *Free energy studies of freezing in slit pores: An order-parameter approach using Monte Carlo simulation*, Mol. Phys. 96 (1999), p. 1249.
[15] J. Bai, J. Wang, and X.C. Zeng, *Multiwalled ice helixes and ice nanotubes*, Proc. Natl. Acad. Sci. USA 103 (2006), p. 19664.
[16] K. Koga, G.T. Gao, X.C. Zeng, and H. Tanaka, *Formation of ordered ice nanotubes inside carbon nanotubes*, Nature 412 (2001), p. 802.
[17] Y. Maniwa, H. Kataura, M. Abe, S. Suzuki, Y. Achiba, H. Kira, and K. Matsuda, *Phase transition in confined water inside carbon nanotubes*, J. Phys. Soc. Jpn. 71 (2002), p. 2863.
[18] K. Koga and H. Tanaka, *Phase diagram of water between hydrophobic surfaces*, J. Chem. Phys. 122 (2005), p. 104711.
[19] C. Alba-Simionesco, B. Coasne, G. Dosseh, G. Dudziak, K.E. Gubbins, R. Radhakrishnan, and M. Sliwinska-Bartkowiak, *Effects of confinement on freezing and melting*, J. Phys. Cond. Matt. 18 (2006), p. R15.
[20] T. Jin, B. Zalar, A. Lebar, M. Vilfan, S. Zumer, and D. Finotello, *Anchoring and structural transitions as a function of molecular length in confined liquid crystals*, Euro. Phys. J.E. 16 (2005), p. 159.
[21] D.B. Zax, D.K. Yang, R.A. Santos, H. Hegemann, E.P. Giannelis, and E. Manias, *Dynamical heterogeneity in nanoconfined poly (styrene) chains*, J. Chem. Phys. 112 (2000), p. 2945.
[22] D. de las Heras, E. Velasco, and L. Mederos, *Effects of wetting and anchoring on capillary phenomena in a confined liquid crystal*, J. Chem. Phys. 120 (2004), p. 4949.
[23] D. de las Heras, E. Velasco, and L. Mederos, *Capillary effects in a confined smectic phase of hard spherocylinders: Influence of particle elongation*, Phys. Rev. E 74 (2006), p. 11709.
[24] R. Guégan, D. Morineau, R. Lefort, A. Moréac, W. Béziel, M. Guendouz, J.M. Zanotti, and B. Frick, *Molecular dynamics of a short-range ordered smectic phase nanoconfined in porous silicon*, J. Chem. Phys. 126 (2007), p. 064902.
[25] G.D. Wall and D.J. Cleaver, *Computer simulation studies of confined liquid–crystal films*, Phys. Rev. E 56 (1997), p. 4306.
[26] T. Gruhn and M. Schoen, *Microscopic structure of molecularly thin confined liquid–crystal films*, Phys. Rev. E 55 (1997), p. 2861.
[27] J. Quintana, E.C. Poire, H. Dominguez, and J. Alejandre, *Phase equilibria of confined liquid crystals*, Mol. Phys. 100 (2002), p. 2597.
[28] D. Micheletti, L. Muccioli, R. Berardi, M. Ricci, and C. Zannoni, *Effect of nanoconfinement on liquid–crystal polymer chains*, J. Chem. Phys. 123 (2005), p. 224705.
[29] H. Steuer, S. Hess, and M. Schoen, *Phase behavior of liquid crystals confined by smooth walls*, Phys. Rev. E 69 (2004), p. 31708.
[30] E. Gwozdz, K. Pasterny, and A. Brodka, *Planar anchoring of polar liquid crystal molecules in slit pore-molecular dynamics simulation study*, Chem. Phys. Lett. 335 (2001), p. 71.
[31] T. Mima and K. Yasuoka, *Interfacial anisotropy in the transport of liquid crystals confined between flat, structureless walls: A molecular dynamics simulation approach*, Phys. Rev. E 77 (2008), p. 11705.
[32] L.F. Rull, J.M. Romero-Enrique, and E.A. Müller, *Observation of surface nematization at the solid-liquid crystal interface via molecular simulation*, J. Phys. Chem. 111 (2007), p. 15998.
[33] E. de Miguel and C. Vega, *The global phase diagram of the Gay–Berne model*, J. Chem. Phys. 117 (2002), p. 6313.
[34] J. Ilnytskyi and M.R. Wilson, *A domain decomposition molecular dynamics program for the simulation of flexible molecules with an arbitrary topology of Lennard–Jones and/or Gay–Berne sites*, Comp. Phys. Comm. 134 (2001), p. 23.
[35] J.G. Gay and B.J. Berne, *Modification of the overlap potential to mimic a linear site-site potential*, J. Chem. Phys. 74 (1981), p. 3316.
[36] T. Miyazaki and M. Yamashita, *Formation of surface stabilised smectic phases driven by electric field under homogeneous anchoring*, Mol. Cryst. Liq. Cryst. A 347 (2000), p. 189.
[37] T.L. Hill, *Statistical mechanics of multimolecular adsorption, I*, J. Chem. Phys. 16 (1948), p. 181.
[38] T. Gruhn and M. Schoen, *Substrate-induced order in confined nematic liquid–crystal films*, J. Chem. Phys. 108 (1998), p. 9124.
[39] M.P. Allen and D.J. Tildesley, *Computer Simulation of Liquids*, Oxford University Press, Oxford, 1987.

[40] P.M. Chaikin and T.C. Lubensky, *Principles of Condensed Matter Physics*, Cambridge, University Press, Cambridge, 1995.
[41] P.G. de Gennes and J. Prost, *The Physics of Liquid Crystal*, Oxford University Press, Oxford, 1993.
[42] M. Dijkstra, R. Roij, and R. Evans, *Wetting and capillary nematization of a hard-rod fluid: A simulation study*, Phys. Rev. E 63 (2001), p. 51703.
[43] Y. Trukhina and T. Schilling, *Computer simulation study of a liquid crystal confined to a spherical cavity*, Phys. Rev. E 77 (2008), p. 11701.
[44] F. Barmes and D.J. Cleaver, *Using particle shape to induce tilted and bistable liquid crystal anchoring*, Phys. Rev. E 71 (2005), p. 21705.

Appendix

In order to compare the orientational order of particles in the slit to one for the bulk system, the 3DMOCF was calculated. In the case of the 3-dimensional system, 3DMOCF is a function of the 3-dimensional distance, r, not r_{2D}. First, $n(r)$ was defined as the number of particles between $(r, r + \Delta r)$, Next, $n(r)$ was given by

$$n(r) = \left\langle \frac{1}{N_{\text{sample}}} \sum_{i=1}^{N_{\text{sample}}} \sum_{j \in \{j \neq i, C_r\}} 1 \right\rangle, \tag{22}$$

where N_{sample} is the number of particles of ith particles in one timestep, and C_r is the region between spheres with the radius of r and $r + \Delta r$. 3DMOCF, $h(r)$, is then defined as

$$h(r) = \frac{1}{n(r)} \left\langle \frac{1}{N_{\text{sample}}} \cdot \sum_{i=1}^{N_{\text{sample}}} \sum_{j \in \{j \neq i, C_r\}} \left(2\cos^2 \theta_{ij} - 1\right) \right\rangle. \tag{23}$$

We defined that $h(r)$ is 0 when no particle is between $(r, r + \Delta r)$.

The system of 27,000 Gay–Berne particles was prepared. The parameters of the potential are the same for confined particles. A periodic boundary condition is imposed in the x-, y- and z-directions. Particles are equilibrated by the constant pressure and temperature ensemble [34]. The pressure is set to 4.5. Five temperatures are investigated; 1.20, 1.15, 1.10, 1.05 and 1.00. At each temperature, we have confirmed that the particles exhibit isotropic, isotropic, nematic, nematic and solid behaviour, respectively. The values of the 3DOP after equilibration are 0.01, 0.03, 0.59, 0.68 and 0.92, respectively.

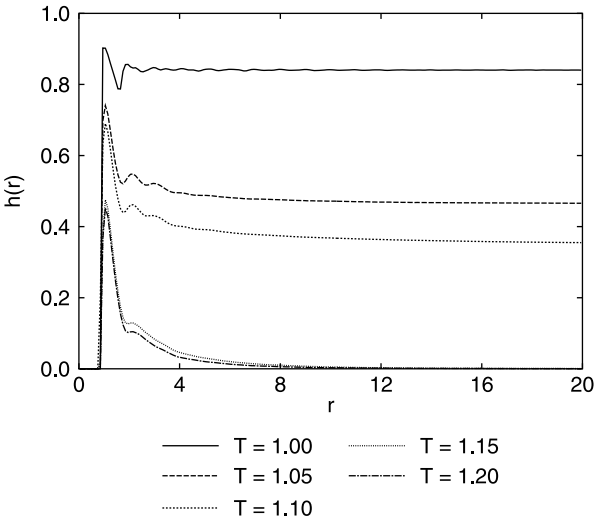

Figure 9. 3-dimensional mutual orientational correlation function (3DMOCF), $h(r)$.

Figure 9 shows 3DMOCF calculated at fire temperatures. When $T = 1.20$ and 1.15, $h(r)$ has a peak around $r \simeq 1$, suddenly decays and then converges under 0.1 and over $r = 3$. It is found that the local order reaches only to the most neighbouring particles in the case of the isotropic particles. When $T = 1.10$ and 1.05, $h(r)$ has a local maximum at $r \simeq 1$; its value is higher than one in the isotropic phase. The tail of $h(r)$ converges to a finite value of 0.36 at $T = 1.10$ and 0.47 at $T = 1.05$. The global uniaxiality of the nematic property is exactly observed at $T = 1.10$ and 1.05. Finally, $h(r)$ at $T = 1.00$ shows the highest uniaxial order. $h(r)$ hardly decays over $r > 0.2$ and maintains the value over 0.84 to the terminal distance of $r = 20.0$. Compared with the above result of the bulk Gay–Berne particles system, the most characteristic property of the system of particles in the flat, structureless slit is that the weak local orientational order decays rather gradually at the high temperatures.